

SPURRITE, TILLEYITE AND ASSOCIATED MINERALS IN THE EXOSKARN ZONE FROM CORNET HILL (METALIFERI MASSIF, APUSENI MOUNTAINS, ROMANIA)

ȘTEFAN MARINCEA[§], DELIA-GEORGETA DUMITRAȘ, NICOLAE CĂLIN, AND ANGELA MARIA ANASON

Department INI, Geological Institute of Romania, 1 Caransebeș Str., RO-012271, Bucharest, Romania

ANDRÉ MATHIEU FRANSOLET AND FRÉDÉRIC HATERT

Laboratoire de Minéralogie, Université de Liège, Sart-Tilman, Bâtiment B 18, B-4000 Liège, Belgium

ABSTRACT

The high-temperature skarn of Cornet Hill (Apuseni Mountains, Romania) is known as one of the rare occurrences of spurrite and tilleyite worldwide. Both minerals concentrate in the outer skarn zone, corresponding to the exoskarn, at the contact between a monzodiorite-quartz monzonite body of Upper Cretaceous age and Tithonic-Kimmeridgian reef limestones. The Cornet Hill skarn is clearly zoned. The zoning is defined by the predominance of series of mineral species and is, from the outer to the inner part of the metasomatic area, as follows: calcite (marble), tilleyite, spurrite, wollastonite + gehlenite + vesuvianite, wollastonite + grossular, quartz monzonite. The exoskarn is confined to the tilleyite- and spurrite-bearing zones. The mineral associations identified in the exoskarn zone so far include: (1) metasomatic or primary products such as spurrite, tilleyite, and accessory gehlenite, grossular, titanian andradite, monticellite, wollastonite, perovskite, vesuvianite, ellestadite-(OH), and (2) hydrothermal and weathering (secondary) minerals such as afwillite, fukalite, scawtite, thaumasite, hibschite, xonotlite, thomsonite, gismondine, plombièrite, tobermorite, riversideite, portlandite, allophane, calcite, and aragonite. Chemical, optical, infrared absorption, and X-ray powder analyses of the primary mineral species, as well as of three secondary species firstly described in the Romanian skarns, *i.e.*, afwillite, thaumasite, and fukalite, are reported here.

Keywords: High-temperature exoskarn, mineral data, tilleyite, spurrite, wollastonite, perovskite, monticellite, ellestadite-OH, afwillite, thaumasite, fukalite, Cornet Hill, Romania.

INTRODUCTION

The high-temperature skarn occurrence of Cornet Hill (Apuseni Mountains, Romania) was first described by Istrate *et al.* (1978) and is known as one of the rare occurrences of spurrite and tilleyite worldwide (Marincea *et al.* 2001, Pascal *et al.* 2001, Grice 2005). To date, only 25 occurrences of spurrite and no more than 15 occurrences of tilleyite have been reported in high-temperature calcic skarns worldwide (Reverdatto 1970, Deer *et al.* 1986, Piret 1997, Pascal *et al.* 2001, and references therein). Beside spurrite and tilleyite, the Cornet Hill occurrence yielded a large array of interesting mineral species, whose detailed inventory was recently given by Marincea *et al.* (2011).

Both spurrite and tilleyite from Cornet Hill are concentrated in the outer skarn zone, corresponding to the exoskarn. Their unusual abundance in two nearly

monomineralic bands clearly defines metasomatic zoning, first observed and described by Istrate *et al.* (1978), who referred to the spurrite- and tilleyite-bearing zones as CH 2 and CH 3, respectively. The mineral assemblage of the two zones was described by Marincea *et al.* (2001) and reveals the overlap of a series of depositional stages and parageneses. Preliminary data on the mineral species described below were given in the same paper (Marincea *et al.* 2001), whereas a petrogenetic approach was undertaken in the study of Pascal *et al.* (2001). For simplicity in the general location of the samples, this work refers to the original zoning proposed by Istrate *et al.* (1978).

This study is of particular interest not only because of the rarity and unusual crystallinity of spurrite and tilleyite from Cornet Hill, but also because of the very clear relationships between them and the “accessory” skarn minerals in the CH 2 and CH 3 zones (*i.e.*,

[§] E-mail address: marincea@igr.ro

perovskite, ellestadite-(OH), calcic garnet, gehlenite, monticellite, and wollastonite). Note also that Grice (2005) used samples from Cornet Hill for refining the crystal structures of tilleyite and spurrite. Details on the mineral chemistry, physical and unit cell parameters, and infrared behavior of the two minerals seems, for this reason, highly desirable. The important abundance of the "accessories" also prompted their precise study, reported in this paper.

GEOLOGICAL SETTING

The Cornet Hill area is located approximately 20 km west of Brad and 40 km northwest of Deva. Geological sketches of the location are given by Istrate *et al.* (1978), Marincea *et al.* (2001), and Pascal *et al.* (2001). The high temperature skarn occurrence herein contains essentially spurrite-, tilleyite-, and gehlenite-bearing skarns that developed at the contact of a monzodiorite - quartz monzonite body of Upper Cretaceous age (Ștefan *et al.* 1988). The skarn protolith consisted of Tithonic-Kimmeridgian reef limestones (in fact, micritic reef limestones with clastic interlayers) of the Căpâlnaș-Techeș unit (Lupu *et al.* 1993).

As mentioned before, the skarn from Cornet Hill is clearly zoned. The zoning described by Istrate *et al.* (1978) is, from the outer to the inner part of the metasomatic area, as follows: calcite (marble), tilleyite, spurrite, wollastonite + gehlenite + vesuvianite, quartz monzonite. Pascal *et al.* (2001) described this zoning in greater detail and distinguished an endoskarn wollastonite-grossular zone at the contact of the intrusive body.

The aim of this study is to investigate from a mineralogical point of view the spurrite- and tilleyite-bearing skarns of the exoskarn zone. The mineral assemblage identified so far includes gehlenite, spurrite, tilleyite, diopside, grossular, titanian andradite, magnetite, monticellite, wollastonite, perovskite, vesuvianite, ellestadite-(OH), calcite, aragonite, pyrrhotite, scawtite, thaumasite, clinocllore, chrysotile, hibschite, xonotlite, thomsonite, gismondine, plombièreite, tobermorite, riversideite, portlandite, and allophane (Marincea *et al.* 2001, Pascal *et al.* 2001). Our efforts will be directed to the characterization of the primary parageneses, without focusing too much on the late metasomatic, hydrothermal, and weathering products, which have been better described in a previous work by Marincea *et al.* (2001). Additional information concerning the mineral assemblages in the Cornet Hill skarn, and particularly on the textural and paragenetic relations between the various phases, was given by Marincea *et al.* (2001) and Pascal *et al.* (2001).

ANALYTICAL PROCEDURES

Electron-microprobe analyses (EMPA) were carried out using a fully-automated CAMECA SX-50 electron

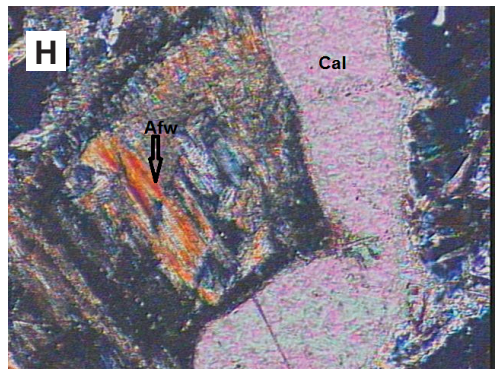
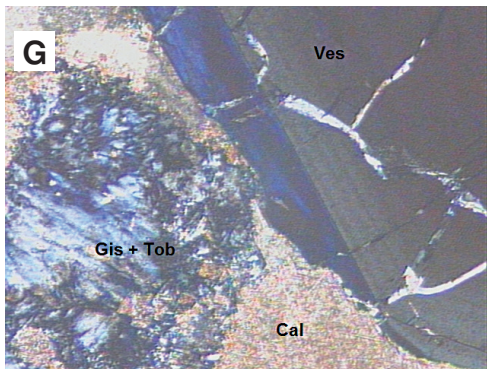
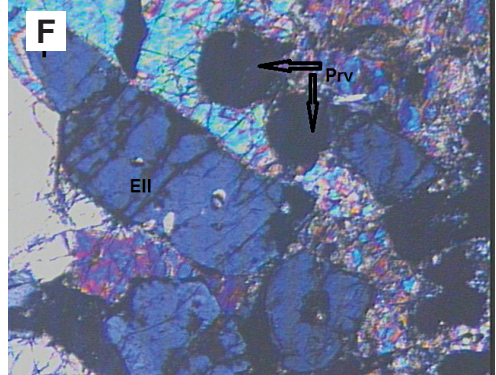
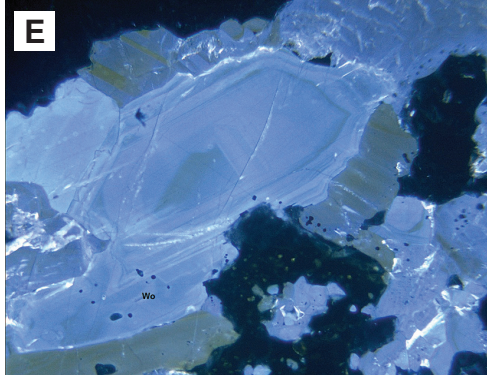
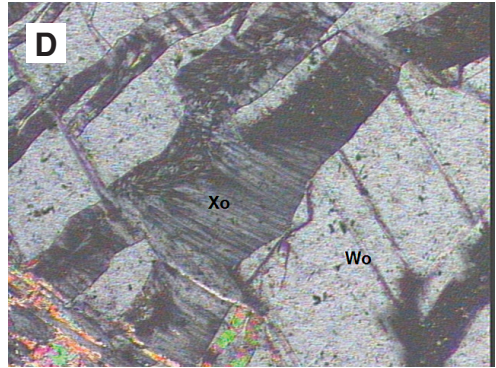
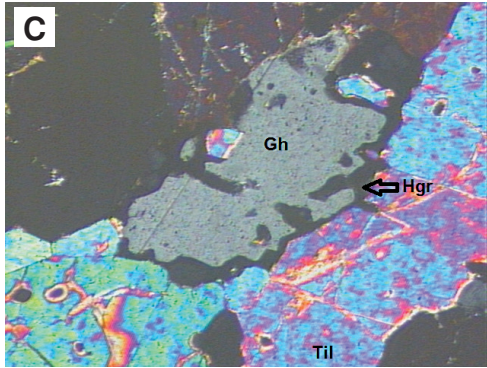
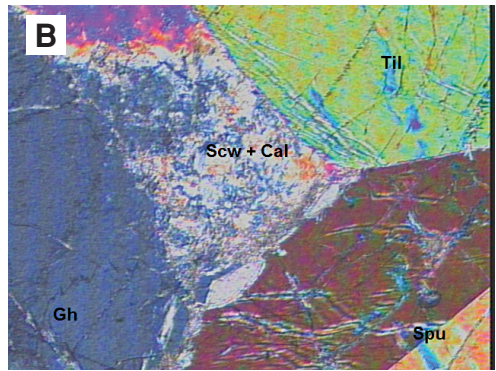
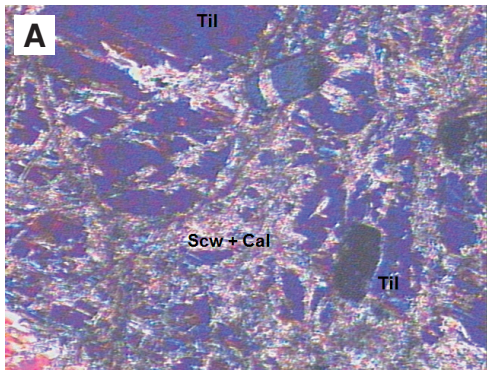
microprobe operated in the wavelength-dispersive mode at Université Pierre et Marie Curie (Paris VI). The standards and operating cautions were the same as described by Marincea *et al.* (2001). Data reduction was done using the PAP correction procedure (Pouchou & Pichoir 1985). The estimated accuracy of the analytical data is $\pm 1\%$ of the amount present. In tilleyite and spurrite the carbon content was calculated assuming stoichiometry.

A wet-chemical analysis was carried out on a selected sample of spurrite using a set of standard methods of quantitative analysis (gravimetry, colorimetry, and absorption spectrometry).

Part of the X-ray powder-diffraction (XRD) analysis was performed on a Siemens D-5000 Kristalloflex automated diffractometer equipped with a graphite diffracted-beam monochromator (CuK α radiation, $\lambda = 1.54056 \text{ \AA}$). The operating conditions were the same as described by Marincea *et al.* (2001). Other analyses were performed using a Bruker (AXS) D8 Advance diffractometer, with the same operating conditions. In both cases, synthetic silicon (NBS 640b) was used as an external standard in order to verify the accuracy of the measurements. The unit-cell parameters were calculated by least-squares refinement of the XRD data using the computer program of Appleman & Evans (1973), modified by Benoit (1987). The full set of X-ray powder data is available from the first author upon request.

Fourier-transform infrared attenuated total reflectance (FTIR-ATR) spectra were recorded from powders of spurrite and tilleyite using a BIORAD FTS 60 (DIGILAB) spectrometer with a Harrick diffuse reflectance device, in the frequency range between 400 and 4000 cm^{-1} . The records were also made using a coupled thermal chamber operated at a heating rate of 10 $^{\circ}\text{C}/\text{min}$, under a constant flow of argon (5 mL/min), between 25 and 800 $^{\circ}\text{C}$. The curve fitting was done using the GRAMS program of Galactic Instruments.

FIG. 1. Photomicrographs showing characteristic relationships between minerals in the exoskarn from Cornet Hill. Excepting (E), transmitted light, crossed nicols. Width of the field = 2.6 mm. (A) Tilleyite (Til) mass, cut by fractures filled with scawtite (Scw) and calcite (Cal). CH 3 zone. (B) Twinned crystal of spurrite (Spu) with tilleyite and gehlenite (Gh). Border between CH 2 and CH 3 zones. (C) Gehlenite surrounded and engulfed by hydrogrossular (Hgr) in the tilleyite mass. CH 3 zone. (D) Xonotlite (Xo) in a zone of parting that breaks up a crystal of wollastonite (Wo). CH 3 zone. (E) Cathodoluminescence photomicrograph showing a zoned crystal of wollastonite. CH 3 zone. (F) Crystals of ellestadite-(OH) (Eil) and perovskite (Prv) in the tilleyite mass. CH 3 zone. (G) Crystal of vesuvianite (Ves) with anomalous birefringence border at the limit with the altered tilleyite. Sheave-like aggregates of gismondine (Gis) and tobermorite (Tob) beside calcite line a fracture that separate the vesuvianite crystal from the tilleyite mass. CH 3 zone. (H) Afwillite (Afw) and calcite on a fracture affecting the spurrite mass. CH 2 zone.



Cathodoluminescence (CL) analyses were performed on thin sections using a Technosyn 8200 Mark II cold-cathode electron gun mounted on a polarizing microscope. The electron beam was accelerated at 10-15 kV, with a 400-500 mA beam current.

The indices of refraction were determined using a conventional JENAPOL-U petrographic microscope with a spindle stage and calibrated immersion liquids (Cargille or temperature-calibrated oils) with a 590 nm interference filter.

DATA FOR PRIMARY MINERALS

Tilleyite

At Cornet Hill, tilleyite is one of the most abundant silicate phases. As shown by Istrate *et al.* (1978), the mineral represents the main constituent of the outer zone of the high-temperature skarn ("the tilleyite zone"), which grades inward into the spurrite zone (CH 2). In this outer zone (CH 3), tilleyite is segregated into essentially monomineralic "orbicules" up to 5 cm² in size. Tilleyite in massive aggregates ("orbicules") seems generally unaltered, but a close examination shows that many crystals are rimmed or penetrated in fissures by scawtite and calcite (Fig. 1A). In hand specimen, the mineral is bluish gray to dark gray and is cross-cut by a web-like network of very thin (up to 2 mm) white

veinlets. On microscopic examination, the vein system is found to contain calcite, scawtite, and some optically indeterminate "cryptocrystalline" phases that proved to be a mixture of calcite, plumbièrite, and tobermorite or riversideite (Marincea *et al.* 2001).

The density of a selected sample of tilleyite (sample 2300), measured by suspension in methylene iodide diluted with toluene, is 2.87(1) g/cm³, which agrees well with the calculated density of 2.867 g/cm³, based on the average chemistry in Table 1 and on the mean cell volume in Table 2. The indices of refraction measured for the same sample are α 1.609(2), β 1.631(2), and γ 1.652(3). The mineral is optically positive, with $2V$ (measured) = 87.5°, which perfectly matches with the calculated value ($2V_{\text{calc}} = 87.53^\circ$).

Chemical data for a representative suite of samples of tilleyite are presented in Table 1. Electron-microprobe studies reveal little variation in the compositions within individual samples, which parallels the behavior of spurrite. No chemical zoning may be observed within the individual crystals. Consequently, the compositions in Table 1 represent averages of many single point analyses within the same thin section.

The structural formulae were calculated on the basis of 13 oxygen atoms, assuming the stoichiometry for the CO₂ content (with SiO₂/CO₂ molar ratios of 1/1). The mineral shows slight departures from ideal stoichiometry. The main deviation is shown by the sums of

TABLE 1. REPRESENTATIVE ELECTRON-MICROPROBE COMPOSITIONS OF TILLEYITE, CORNET HILL*

Sample	P 49	P 55	2159	2162	2170	2173	2175	2176	2233	2265	2300	2305	2310	2315
N ⁽¹⁾	3	3	12	10	9	20	4	3	15	11	11	5	3	6
SiO ₂	25.31	25.04	23.97	24.73	24.06	23.97	24.16	24.53	24.48	24.98	25.02	23.98	24.58	23.70
TiO ₂	0.01	0.00	0.00	0.03	0.05	0.03	0.09	0.00	0.05	0.06	0.01	0.00	0.03	0.07
Al ₂ O ₃	0.02	0.01	0.00	0.00	0.00	0.00	0.00	0.00	0.00	0.00	0.00	0.00	0.00	0.02
FeO ⁽²⁾	0.04	0.01	0.05	0.29	0.04	0.04	0.04	0.04	0.04	0.01	0.02	0.06	0.00	0.02
MgO	0.07	0.07	0.02	0.03	0.02	0.03	0.05	0.03	0.03	0.03	0.03	0.03	0.04	0.03
MnO	0.02	0.03	0.03	0.04	0.02	0.04	0.03	0.05	0.02	0.02	0.01	0.00	0.06	0.02
CaO	59.75	58.53	55.01	58.51	57.57	54.95	56.32	58.39	57.97	57.55	57.39	54.60	57.53	55.63
Na ₂ O	0.01	0.00	0.01	0.02	0.01	0.01	0.01	0.01	0.01	0.01	0.01	0.02	0.00	0.01
K ₂ O	0.00	0.00	0.00	0.01	0.00	0.00	0.02	0.02	0.00	0.01	0.00	0.00	0.01	0.01
CO ₂ ⁽³⁾	18.54	18.34	17.56	18.12	17.62	17.56	17.70	17.97	17.93	18.30	18.33	17.56	18.00	17.36
Total	103.77	102.02	96.65	101.78	99.39	96.63	98.42	101.04	100.50	100.98	100.87	96.18	100.27	96.90
Number of cations on the basis of 13 (O)														
Si	1.989	1.997	2.011	1.985	1.979	2.011	1.997	1.983	1.987	2.007	2.011	2.018	1.995	1.992
Ti	0.001	0.000	0.000	0.002	0.003	0.002	0.006	0.000	0.003	0.004	0.001	0.000	0.002	0.004
Al	0.002	0.001	0.000	0.000	0.000	0.000	0.000	0.000	0.000	0.000	0.000	0.000	0.000	0.002
Fe ²⁺	0.003	0.001	0.004	0.019	0.003	0.003	0.003	0.003	0.001	0.001	0.004	0.000	0.001	0.004
Mg	0.008	0.007	0.003	0.004	0.002	0.004	0.006	0.004	0.004	0.004	0.004	0.005	0.004	0.003
Mn	0.001	0.002	0.002	0.003	0.001	0.003	0.002	0.003	0.001	0.001	0.001	0.000	0.004	0.001
Ca	5.029	5.001	4.945	5.030	5.073	4.940	4.987	5.057	5.041	4.955	4.943	4.923	5.004	5.010
Na	0.002	0.000	0.002	0.003	0.002	0.002	0.002	0.002	0.002	0.002	0.003	0.000	0.002	0.003
K	0.000	0.000	0.000	0.001	0.000	0.000	0.002	0.002	0.000	0.001	0.000	0.000	0.001	0.001
C	1.989	1.997	2.011	1.985	1.979	2.011	1.997	1.983	1.987	2.007	2.011	2.018	1.995	1.992
Σ cat.	9.024	9.006	8.978	9.032	9.042	8.976	9.002	9.037	9.026	8.982	8.978	8.964	9.008	9.012

* Results expressed in wt.%; (1) number of point analyses; (2) total iron as FeO; (3) as calculated for stoichiometry.

TABLE 2. CRYSTALLOGRAPHIC PARAMETERS OF SELECTED MINERALS IN THE CORNET HILL EXOSKARN

Mineral	System	Space group	Sample	Zone	a (Å)	b (Å)	c (Å)	β (°)	V (Å ³)	n ⁽¹⁾	N ⁽²⁾	2 θ range ⁽³⁾ (°)
tilleyite	M	<i>P2₁/a</i>	P 11	CH 3	15.036(16)	10.263(8)	7.550(9)	104.49(8)	1128.0(7)	6	43	10 - 60
tilleyite	M	<i>P2₁/a</i>	P 49	CH 2	15.142(5)	10.281(2)	7.570(9)	105.20(1)	1137.2(3)	8	41	10 - 60
tilleyite	M	<i>P2₁/a</i>	2162	CH 3	15.123(6)	10.252(3)	7.583(3)	105.20(2)	1134.5(4)	6	45	10 - 60
tilleyite	M	<i>P2₁/a</i>	2223	CH 3	15.099(9)	10.247(5)	7.576(4)	105.11(3)	1131.6(4)	4	41	10 - 60
tilleyite	M	<i>P2₁/a</i>	2300	CH 2	15.074(5)	10.238(3)	7.573(3)	105.09(2)	1128.4(5)	6	53	10 - 60
tilleyite	M	<i>P2₁/a</i>	2301	CH 3	15.096(8)	10.241(5)	7.576(4)	105.17(3)	1130.4(7)	5	87	10 - 60
tilleyite	M	<i>P2₁/a</i>	2315	CH 3	15.121(8)	10.258(6)	7.579(4)	105.23(3)	1134.3(8)	4	85	10 - 60
tilleyite	M	<i>P2₁/a</i>	N 10	CH 3	15.089(9)	10.247(8)	7.604(6)	105.26(4)	1134.3(9)	8	61	10 - 60
tilleyite	M	<i>P2₁/a</i>	S 2 a	CH 2	15.104(4)	10.247(3)	7.576(2)	105.09(1)	1132.0(4)	7	106	10 - 60
tilleyite	M	<i>P2₁/a</i>	S 2 c	CH 2	15.130(5)	10.256(3)	7.584(2)	105.17(2)	1135.7(5)	9	64	10 - 60
spurrite	M	<i>P2₁/a</i>	P 49	CH 2	10.515(5)	6.728(3)	14.203(6)	101.40(2)	985.0(1)	5	40	10 - 60
spurrite	M	<i>P2₁/a</i>	2160	CH 2	10.489(3)	6.714(2)	14.165(4)	101.26(1)	978.4(3)	10	78	10 - 80
spurrite	M	<i>P2₁/a</i>	2176 a	CH 2	10.492(2)	6.709(1)	14.166(3)	101.32(1)	977.7(2)	10	74	10 - 80
spurrite	M	<i>P2₁/a</i>	2237	CH 2	10.491(5)	6.698(3)	14.175(7)	101.33(3)	976.6(6)	5	87	10 - 80
spurrite	M	<i>P2₁/a</i>	2300	CH 2	10.490(7)	6.708(5)	14.186(9)	101.41(5)	978.6(9)	7	38	10 - 80
spurrite	M	<i>P2₁/a</i>	N 2	CH 2	10.492(6)	6.705(3)	14.171(7)	101.30(3)	977.6(6)	5	97	10 - 80
spurrite	M	<i>P2₁/a</i>	N 4	CH 2	10.481(4)	6.713(2)	14.174(6)	101.34(2)	977.8(5)	6	79	10 - 80
gehlenite	Q	<i>P4₂/m</i>	2160	CH 2	7.684(3)	-	5.061(2)	-	298.8(4)	5	42	15 - 90
gehlenite	Q	<i>P4₂/m</i>	2301	CH 3	7.728(1)	-	5.044(1)	-	301.2(5)	9	50	10 - 80
gehlenite	Q	<i>P4₂/m</i>	2315	CH 3	7.696(3)	-	5.058(2)	-	299.5(2)	5	48	10 - 80
grossular	C	<i>Ia3d</i>	2233	CH 3	11.888(1)	-	-	-	1680.0(6)	3	25	20 - 90
wollastonite	M	<i>P2₁/a</i>	P 11	CH 3	15.456(6)	7.327(4)	7.081(3)	95.34(2)	798.4(3)	10	64	10 - 80
wollastonite	M	<i>P2₁/a</i>	2233	CH 3	15.410(5)	7.321(3)	7.066(2)	95.31(2)	793.7(2)	7	80	10 - 80
wollastonite	M	<i>P2₁/a</i>	2305	CH 3	15.400(5)	7.318(3)	7.061(2)	95.31(2)	792.3(3)	4	94	10 - 80
wollastonite	M	<i>P2₁/a</i>	2315	CH 3	15.401(3)	7.325(1)	7.069(1)	95.41(1)	794.0(2)	9	79	10 - 80
wollastonite	M	<i>P2₁/a</i>	N 10	CH 3	15.412(5)	7.324(3)	7.069(2)	95.31(2)	794.5(3)	5	81	10 - 80
perovskite	O	<i>Pbnm</i>	N 4	CH 2	5.381(5)	5.426(6)	7.648(7)	-	223.3(3)	3	35	20 - 70
perovskite	O	<i>Pbnm</i>	2160	CH 2	5.382(3)	5.437(3)	7.634(4)	-	223.4(1)	4	43	20 - 70
perovskite	O	<i>Pbnm</i>	CH 78	CH 3	5.376(1)	5.436(1)	7.642(2)	-	223.3(1)	10	39	20 - 70
ellestadite-OH	H	<i>P6₃/m</i>	2173	CH 2	9.491(3)	-	6.930(2)	-	540.5(3)	3	20	10 - 65
fukalite	O	<i>Bmmb</i>	P 49	CH 2	5.498(7)	3.798(3)	23.407(19)	-	487.7(7)	3	15	20 - 55
afwillite	M	<i>Cc</i>	2160	CH 2	16.279(6)	5.631(2)	13.230(5)	134.80(1)	860.6(4)	10	114	10 - 80
thaumasite	H	<i>P6₃/m</i>	T 2 d	CH 2	11.031(3)	-	10.402(4)	-	1096.2(5)	9	99	5 - 80

(1) Number of refining cycles; (2) number of reflections used for refinement; (3) range of 2 θ angles used for collecting reflections.

6-, 7-, and 8-fold coordinated cations (see Grice 2005 for the structure), which are generally slightly higher than 5 *apfu* (atoms per formula unit), whereas the sums of tetrahedral cations are generally lower than 2 *apfu*. The (Mg, Mn, Fe)-for-Ca substitutions are very limited; only up to 0.52% of the octahedral sites are occupied by cations other than Ca.

X-ray powder diffraction patterns of about 20 samples of tilleyite from Cornet Hill were recorded in order to select the best to be used to calculate the cell parameters. The primary patterns are available upon request from the first author. The cell parameters were successfully refined based on a monoclinic *P2₁/a* cell (Smith 1953, Louisnathan & Smith 1970, Grice 2005), after indexing the patterns in analogy with PDFs 71-2079 and 73-2117. Sets of 41 to 87 reflections in the 2 θ range between 10 and 60° (CuK α , λ = 1.54056 Å) for which unambiguous indexing was possible, were used to refine the cell dimensions, from which the

most representative are summarized in Table 2. The cell parameters in the table agree fairly well with the values refined for tilleyite from the same locality by Grice (2005), *i.e.*, *a* 15.082(3), *b* 10.236(2), *c* 7.572(1) Å and β 105.17(1)°. The “layered” structure of tilleyite, however, permits strong departures from the average cell parameters due to the different degrees of polymerization of the silicate groups in the structure (Grice 2005). The variability of the cell parameters of tilleyite, in spite of the very slight variation in the chemical composition, can be observed by comparing the cell parameters published by Smith (1953) with the data inventory of Rubenach & Cuff (1985), and is obvious for the samples from Cornet Hill.

Infrared data for tilleyite are scarce and, consequently, infrared attenuated (FTIR-ATR) spectra were acquired for a representative sample. The position of the bands is better depicted in Table 3, whereas Figure 2 reveals the evolution with temperature of the character

TABLE 3. POSITIONS AND ASSIGNMENTS OF THE INFRARED ABSORPTION BANDS RECORDED FOR A SELECTED SAMPLE OF TILLEYITE FROM CORNET HILL *

Structural group	Vibrational mode	Wavenumber (cm ⁻¹)	Character, intensity ⁽²⁾
(OH) ⁻ (1)	O-H-O stretching (weak hydrogen bond)	3589	sh, w
H ₂ O (2)	H-O-H stretching	3414	b, w
(OH) ⁻ (1)	O-H-O stretching (strong hydrogen bond)	2982	sh, m
(OH) ⁻ (1)	O-H-O stretching (strong hydrogen bond)	2874	sh, m
(CO ₃) ²⁻ (3)	overtone of the ν_2 out-of-plane bending	2571	sh, m
(CO ₃) ²⁻ (3)	multiphonon band ($\nu_1 + \nu_3$)	2511	sh, s
(CO ₃) ²⁻ (3)	multiphonon band ($\nu_3 + \nu_4$)	2140	sh, w
(CO ₃) ²⁻ (3)	overtone of the ν_2 out-of-plane bending or ($\nu_1 + \nu_4$)	1795	sh, s
H ₂ O (2)	H-O-H "scissors" bending	1653	shd, w
(CO ₃) ²⁻ (3)	ν_3 antisymmetric stretching	1438	sh, vs
(CO ₃) ²⁻ (3)	ν_3' antisymmetric stretching	1402	shd, vs
(CO ₃) ²⁻ (3)	multiphonon band ($\nu_1 + \nu_7^{(4)}$)	1180	sh, w
(CO ₃) ²⁻ (3)	multiphonon band ($\nu_1 + \nu_7^{(4)}$)	1163	sh, w
(CO ₃) ²⁻ (3)	multiphonon band ($\nu_1 + \nu_7^{(4)}$)	1093	sh, w
(CO ₃) ²⁻ (3)	ν_1 symmetric stretching	1080	sh, w
(Si ₂ O ₇) ⁶⁻	ν_3 antisymmetric stretching Si-O-Si	1023	sh, m
(Si ₂ O ₇) ⁶⁻	ν_3 antisymmetric stretching Si-O	967	sh, m
(Si ₂ O ₇) ⁶⁻	ν_3' antisymmetric stretching Si-O	926	sh, m
(Si ₂ O ₇) ⁶⁻	ν_1 symmetric stretching Si-O	907	sh, w
(CO ₃) ²⁻ (3)	ν_2 out-of-plane bending	877	sh, vs
(Si ₂ O ₇) ⁶⁻	ν_1' symmetric stretching Si-O		
(CO ₃) ²⁻ (3)	satellite of ν_2 out-of-plane bending	848	sh, m
(CO ₃) ²⁻ (3)	ν_4 in-plane bending	713	sh, s
(CO ₃) ²⁻ (3)	ν_4' in-plane bending	699	sh, w
(Si ₂ O ₇) ⁶⁻	ν_1 symmetric stretching Si-O-Si	668	sh, w
(Si ₂ O ₇) ⁶⁻	ν_1' symmetric stretching Si-O-Si	647	sh, w
(Si ₂ O ₇) ⁶⁻	ν_4 in-plane bending Si-O-Si (?)	543	sh, m
(CaO _n) ^{p-} (5)	composed lattice mode + in-plane Si-O-Si bending	489	sh, m
(Si ₂ O ₇) ⁶⁻			
(Si ₂ O ₇) ⁶⁻	ν_4 in-plane bending Si-O	437	sh, m

* Abbreviations represent: s = strong; m = medium; w = weak; vs = very strong; sh = sharp; b = broad; shd = shoulder; (1) due to an admixed, hydroxyl-bearing phase; (2) due to the adsorbed water; (3) bands assignable to (CO₃)²⁻ groups in both tilleyite and admixed calcite; (4) notation according to White (1974); (5) n = 6, 7, 8 and p = 10, 12, 14 accepting the structure proposed by Grice (2005).

and intensity of the absorption bands. A first look shows that the sample is not pure, containing H₂O- and (OH)-bearing phases, identified as scawtite and plombièreite by Marincea *et al.* (2001). Regarding the spectra, a few remarks are considered important:

(1) A broad hump centered at 3414 cm⁻¹, associated with weak absorption at 1653 cm⁻¹, suggests that the analyzed sample contains adsorbed (molecular) water or a hydrous phase (*e.g.*, scawtite), since both bands disappear with heating (Fig. 2).

(2) The bands associated with the O-H...O stretching from the (OH) groups reflect the presence of a secondary phase containing at least three different hydrogen bonds, perfectly compatible with plombièreite.

(3) Many of the bands depicted in Table 3 are assignable to the vibrational modes of the (CO₃)²⁻ group, including overtones and multiphonon bands. These

bands could originate both from tilleyite itself and from admixed calcite, but, apparently, the analyzed material is free from contaminating carbonate. For example, an obvious multiphonon band appears at 1795 cm⁻¹ and could be reasonably assigned to a first rank overtone of the ν_2 out-of-plane bending of the carbonate group or to a multiphonon band induced by ($\nu_1 + \nu_4$) (Ross & Goldsmith 1964). This band has been mentioned both in the IR spectra of carbonates (*e.g.*, Ross & Goldsmith 1964, White 1974) and in the spectra of other compounds containing diorthosilicate and carbonate groups (*e.g.*, biraite, Konev *et al.* 2005).

(4) The presence of the (Si₂O₇)⁶⁻ groups in the structure of tilleyite requires a different treatment for the Si-O bonds, since the vibrations of the Si-O-Si bonds involving the apical oxygen must be treated separately from those of the terminal Si-O bonds pertaining to

lateral $(\text{SiO}_3)^{2-}$ groups (Lazarev 1974). Consequently, in Table 3, the vibrations pertaining to the lateral $(\text{SiO}_3)^{2-}$ groups are depicted as Si-O vibrations, whereas the vibrations involving the apical oxygen linking the two SiO_4 tetrahedrons are depicted as Si-O-Si vibrations.

Spurrite

Spurrite is the dominant mineral in the CH 2 zone (90-95 vol.%), where it forms nearly monomineralic

masses of grayish blue to pale gray color. A precise study shows, however, that the typical assemblage is spurrite + perovskite. The spurrite-bearing skarn is characterized by a massive appearance with medium-grained crystals of spurrite that generally exceed 5 mm in their largest dimension, without preferred orientation. The mineral is commonly extremely fresh and is the least altered primary skarn mineral in the area. Some of the larger patches of spurrite are, however, cross cut by microveins containing scawtite, plombièreite,

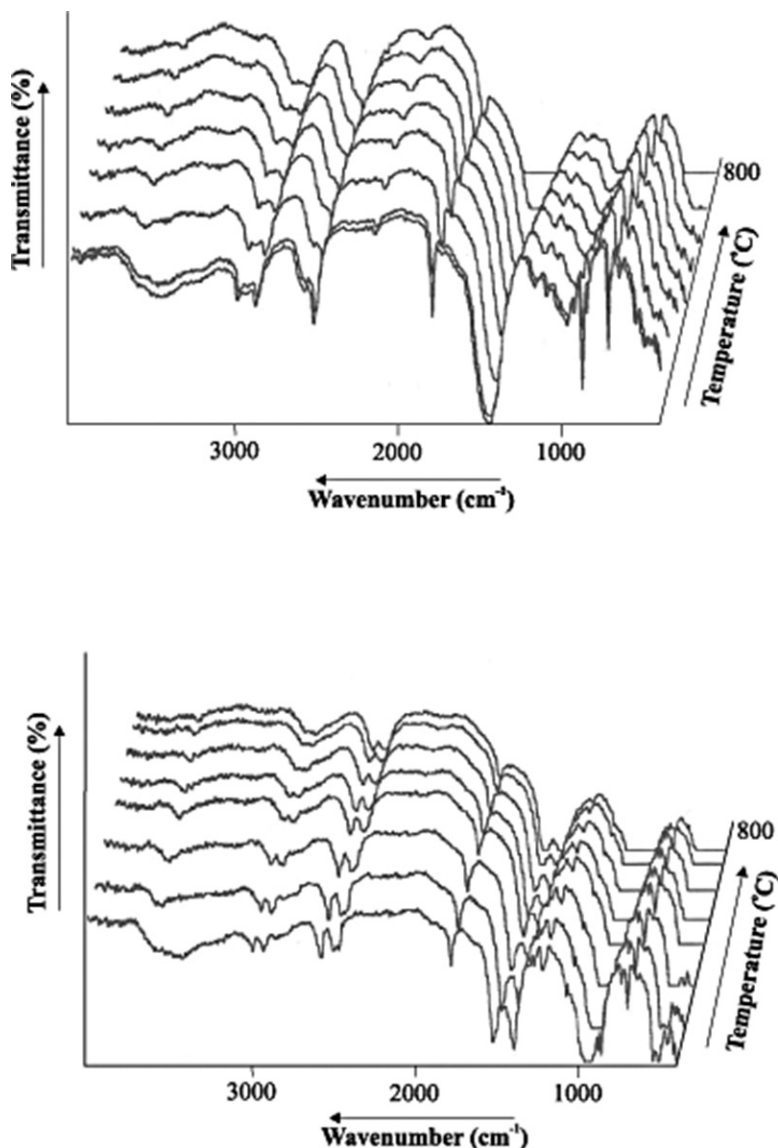


FIG. 2. Thermally-assisted FTIR spectra of selected samples of tilleyite (top) and spurrite (bottom) from Cornet Hill. Heating speed: 10 °C/min, under argon flow.

tobermorite, calcite, and secondary aragonite, or altered by awillite or thaumasite. Similar but more advanced textural features of alteration have been noted for spurrite from other worldwide localities (e.g., Scawt Hill, Tilley 1938).

Spurrite from Cornet Hill shows well-developed simple twinning (Fig. 1B). The 2V angle determined by us (2V = 39°) is slightly smaller than that determined by Tilley (1929) for the spurrite from Scawt Hill (2V = 40°), but is identical to the value measured for this mineral by Istrate *et al.* (1978). The indices of refraction determined for a representative sample (2176 a) are $\alpha = 1.637(2)$, $\beta(\text{calc.}) = 1.675(2)$, and $\gamma = 1.680(3)$. The measured density of the same sample [$D = 3.02(2)$ g/cm³] agrees perfectly with the calculated density ($D_x = 3.022$ g/cm³).

The mean unit-cell parameters obtained as average of the different values in Table 2 are a 10.496(15), b 6.719(8), c 14.182(18) Å, and β 101.38(4)°; they are slightly larger than those given for the sample used for structure refinement by Smith *et al.* (1960) [a 10.49(5), b 6.705(50), c 14.16(5) Å, and β 101.32(8)°], but also for a sample from the same locality, used for structure refinement by Grice (2005) [a 10.484(1), b 6.712(1), c 14.156(2) Å, and β 101.27(1)°].

Crystals of spurrite are unzoned. EMPA of several grains, including core and rim compositions, indicate exceptionally uniform chemistry. This is also reflected by a wet-chemical analysis of a carefully hand-picked separate; except for a slightly higher content of Al, the composition perfectly matches the results of the EMP analyses. The chemical compositions are listed in Table 4. For the EMP analyses, the proportion of CO₂ was deduced assuming a molar ratio SiO₂/CO₂ = 2/1, according to the crystal-structure refinement of Smith *et al.* (1960) and Grice (2005), and all compositions were normalized to 100 wt.%. Unit formulae were normalized to 11 oxygen atoms. As may be seen in Table 4, the total of seven- and eight-fold coordinated cations does not significantly exceed the ideal 5 *apfu* (see Grice 2005 for the structure) and the cation sum approaches the ideally 8 *apfu*. The abundances of Mn (< 0.005 *apfu*), Fe (< 0.005 *apfu*), and Mg (< 0.008 *apfu*) are very low and agree perfectly with those observed in tilleyite.

As in the case of tilleyite, the IR spectra of spurrite are scarce. Consequently, Figure 2 gave FTIR-ATR spectra of a representative sample taken at different temperatures, whereas the assignment of the bands is shown in Table 5. The infrared spectrum of spurrite invokes a few comments, as well.

TABLE 4. CHEMICAL ANALYSES OF SELECTED SAMPLES OF SPURRITE, CORNET HILL*

Sample	P 49	2176A	2176B	2176C	2237	2367	2368	2237 ⁽⁴⁾
N ⁽¹⁾	6	7	5	5	3	3	5	-
SiO ₂	26.77	26.95	26.80	26.86	26.76	26.80	26.89	26.99
TiO ₂	0.01	0.04	0.05	0.01	0.00	0.01	0.01	0.00
Al ₂ O ₃	0.02	0.00	0.00	0.00	0.00	0.02	0.01	0.28
FeO ⁽²⁾	0.06	0.05	0.00	0.02	0.08	0.03	0.01	0.08
MgO	0.03	0.01	0.01	0.01	0.03	0.00	0.00	0.07
MnO	0.02	0.03	0.05	0.08	0.00	0.01	0.01	0.02
CaO	63.21	62.98	63.17	63.10	63.23	63.32	63.21	62.26
Na ₂ O	0.07	0.06	0.09	0.07	0.04	0.00	0.00	0.13
K ₂ O	0.01	0.01	0.01	0.01	0.06	0.00	0.01	0.07
CO ₂ ⁽³⁾	9.80	9.87	9.82	9.84	9.80	9.81	9.85	9.90
Total	100.00	100.00	100.00	100.00	100.00	100.00	100.00	99.80
Number of cations on the basis of 11 (O)								
Si	1.986	1.996	1.988	1.991	1.986	1.988	1.992	1.998
Ti	0.001	0.002	0.003	0.001	0.000	0.001	0.001	0.000
Al	0.002	0.000	0.000	0.000	0.000	0.002	0.001	0.024
Fe ²⁺	0.004	0.003	0.000	0.001	0.005	0.002	0.001	0.005
Mg	0.003	0.001	0.001	0.001	0.003	0.000	0.000	0.008
Mn	0.001	0.002	0.003	0.005	0.000	0.001	0.001	0.001
Ca	5.024	4.997	5.019	5.012	5.028	5.026	5.018	4.939
Na	0.010	0.009	0.013	0.010	0.006	0.000	0.000	0.019
K	0.001	0.001	0.001	0.001	0.006	0.000	0.001	0.007
C	0.993	0.998	0.994	0.996	0.993	0.994	0.996	1.001
∑ cat.	8.025	8.009	8.022	8.018	8.027	8.018	8.011	8.001

* Results expressed in wt.%; (1) number of point analyses; (2) total iron as FeO; (3) in the electron-microprobe analyses, as calculated for an ideal Si/C ratio of 2/1; (4) wet-chemical analysis.

TABLE 5. POSITIONS AND ASSIGNMENTS OF THE INFRARED ABSORPTION BANDS RECORDED FOR A SELECTED SAMPLE OF SPURRITE FROM CORNET HILL *

Structural group	Vibrational mode	Wavenumber (cm ⁻¹)	Character, intensity ⁽²⁾
(OH) ⁻ (1)	O-H-O stretching (weak hydrogen bond)	3732	sh, w
H ₂ O (2)	H-O-H stretching	3592	b, w
(OH) ⁻ (1)	O-H-O stretching (strong hydrogen bond)	2998	sh, m
(OH) ⁻ (1)	O-H-O stretching (strong hydrogen bond)	2926	sh, m
(CO ₃) ²⁻ (3)	overtone of the ν_2 out-of-plane bending	2575	sh, m
(CO ₃) ²⁻ (3)	multiphonon band ($\nu_1 + \nu_3$)	2502	sh, m
(CO ₃) ²⁻ (3)	overtone of the ν_2 out-of-plane bending or ($\nu_1 + \nu_4$)	1779	sh, s
H ₂ O (2)	H-O-H "scissors" bending	1652	sh, w
(CO ₃) ²⁻ (3)	ν_3 + acoustic mode	1520	sh, vs
(CO ₃) ²⁻ (3)	ν_3 antisymmetric stretching	1470	sh, s
(CO ₃) ²⁻ (3)	ν_3 antisymmetric stretching	1398	sh, vs
(CO ₃) ²⁻ (3)	multiphonon band ($\nu_1 + \nu_{14}$) ⁽⁴⁾	1275	sh, m
(CO ₃) ²⁻ (3)	multiphonon band ($\nu_1 + \nu_{10}$) ⁽⁴⁾	1219	sh, m
(CO ₃) ²⁻ (3)	ν_1 symmetric stretching	1080	sh, m
(SiO ₄) ⁴⁻	ν_3 antisymmetric stretching	1054	shd, m
(SiO ₄) ⁴⁻	ν_3 antisymmetric stretching	950	sh, vs
(SiO ₄) ⁴⁻	ν_3 antisymmetric stretching	925	sh, vs
(CO ₃) ²⁻ (3)	ν_2 out-of-plane bending	884	sh, s
(SiO ₄) ⁴⁻	ν_1 symmetric stretching	863	sh, s
(OH) ⁻ (1) (?)	(OH) libration (?)	776	sh, w
(OH) ⁻ (1) (?)	(OH) libration (?)	746	sh, w
(CO ₃) ²⁻ (3)	ν_4 in-plane bending	703	sh, m
(SiO ₄) ⁴⁻	ν_4 in-plane bending	645	sh, w
(SiO ₄) ⁴⁻	ν_4 in-plane bending	542	sh, s
(SiO ₄) ⁴⁻	ν_4 in-plane bending	513	sh, s
(SiO ₄) ⁴⁻	ν_2 out-of-plane bending	451	sh, w

* Abbreviations represent: s = strong; m = medium; w = weak; vs = very strong; sh = sharp; b = broad; shd = shoulder; (1) due to an admixed, hydroxyl-bearing phase; (2) due to the adsorbed water; (3) bands assignable to (CO₃)²⁻ groups in both tilleyite and admixed calcite; (4) notation according to White (1974).

As in the case of tilleyite, admixed OH-bearing and hydrous phases are present in the analyzed material and gave specific stretching bands (Table 5). These bands are practically identical with those recorded for the tilleyite separate, so the comments could be the same.

A large number of the recorded bands could be reasonably assigned to the (CO₃)²⁻ groups in the structure; note that the number of multiphonon bands and overtones is considerably larger.

The multiplicity of the infrared bands assumable to the (SiO₄)⁴⁻ groups (1 ν_1 + 1 ν_2 + 3 ν_3 + 3 ν_4) agrees with a C_{2v} punctual symmetry of these groups.

Gehlenite

Gehlenite is a common constituent in the entire skarn area of Cornet Hill. In the exoskarn zone, the mineral occurs as cluster of crystals isolated in the spurrite- or tilleyite-bearing skarn, which probably indicates a local excess of Al. A more extensive description of the mineral was offered by Marincea *et al.* (2001, 2011), who gives chemical, crystallographic, and physical

data. In many cases, the crystals of gehlenite from the exoskarn are embedded and partially engulfed by vesuvianite or hydrogarnet (Fig. 1C) as a result of a late stage metasomatic event (Marincea *et al.* 2001).

Wollastonite

As shown by Marincea *et al.* (2001) and Pascal *et al.* (2001), wollastonite-2M is rather common in the endoskarn zone (CH 1), where it forms a well-defined and nearly monomineralic subzone. Wollastonite was also found in exoskarn, as veins or remnants hosted by the spurrite or tilleyite masses. In both cases, the mineral is commonly altered along fractures or in patches to very fine-grained material shown to be xonotlite (Fig. 1D) or a mixture of xonotlite and tobermorite.

The refractive indices of a selected sample are $\alpha = 1.608(1)$, $\beta(\text{calc.}) = 1.617(1)$, and $\gamma = 1.618(1)$, for an optical angle $2V_\alpha = 36^\circ$. The mineral has in some cases simple twinning parallel to (100). Both the refraction indices and the low birefringence suggest that the mineral contains low (Fe,Mg)SiO₃ in solid solution,

TABLE 6. REPRESENTATIVE ELECTRON-MICROPROBE COMPOSITIONS OF WOLLASTONITE, CORNET HILL*

Sample	P 57	2157	2163	2167	2362	2363 A	2363 B	2364	P 55	2315	2316	2361	2365	2366
N ⁽¹⁾	3	3	4	3	18	10	14	8	3	3	3	5	12	10
Zone	CH 1	CH 1	CH 1	CH 1	CH 2	CH 2	CH 2	CH 2	CH 3	CH 3	CH 3	CH 3	CH 3	CH 3
SiO ₂	51.21	52.14	51.47	51.56	51.73	51.68	51.72	51.87	51.27	51.48	51.45	51.81	51.83	51.73
Al ₂ O ₃	0.12	0.02	0.11	0.30	0.24	0.20	0.19	0.17	0.15	0.20	0.18	0.20	0.16	0.19
FeO ⁽²⁾	0.00	0.04	0.07	0.03	0.04	0.03	0.04	0.02	0.02	0.05	0.03	0.06	0.05	0.05
MgO	0.11	0.13	0.10	0.10	0.05	0.07	0.06	0.03	0.10	0.06	0.04	0.06	0.05	0.06
MnO	0.05	0.03	0.01	0.03	0.03	0.04	0.04	0.03	0.01	0.04	0.00	0.03	0.03	0.03
CaO	48.38	48.27	47.57	47.89	48.64	48.56	48.71	48.78	48.30	48.01	48.33	48.68	48.67	48.75
Na ₂ O	0.03	0.00	0.00	0.00	0.00	0.00	0.00	0.00	0.00	0.01	0.02	0.00	0.00	0.00
K ₂ O	0.01	0.00	0.00	0.01	0.00	0.00	0.01	0.00	0.00	0.00	0.02	0.00	0.00	0.00
Total	99.91	100.63	99.33	99.92	100.73	100.58	100.77	100.90	99.85	99.85	100.07	100.84	100.79	100.81
Number of cations on the basis of 18 (O)														
Si	5.958	6.005	6.004	5.981	5.964	5.967	5.963	5.970	5.964	5.981	5.970	5.967	5.972	5.962
Al	0.016	0.003	0.015	0.041	0.033	0.027	0.026	0.023	0.021	0.027	0.025	0.027	0.022	0.026
Fe ²⁺	0.000	0.004	0.007	0.003	0.004	0.003	0.004	0.002	0.002	0.005	0.003	0.006	0.005	0.005
Mg	0.019	0.022	0.017	0.017	0.009	0.012	0.010	0.005	0.017	0.010	0.007	0.010	0.009	0.010
Mn	0.005	0.003	0.001	0.003	0.003	0.004	0.004	0.003	0.001	0.004	0.000	0.003	0.003	0.003
Ca	6.031	5.956	5.945	5.952	6.008	6.007	6.017	6.015	6.020	5.976	6.009	6.007	6.008	6.020
Na	0.007	0.000	0.000	0.000	0.000	0.000	0.000	0.000	0.000	0.002	0.004	0.000	0.000	0.000
K	0.001	0.000	0.000	0.001	0.000	0.000	0.001	0.000	0.000	0.000	0.003	0.000	0.000	0.000

* Results expressed in wt.%; (1) number of point analyses; (2) total iron as FeO.

which is fully supported by the chemical analyses in Table 6.

The chemical formula of the mineral is close to the stoichiometry. No major differences were found between the compositions of wollastonite samples from endoskarn (CH 1 zone, also illustrated in Table 6), and from exoskarn (CH 2 and CH 3 zones). A cathodoluminescence zoning of some individual crystals could be observed on exposure to cold-cathode CL (Hans Peter Schertl, pers. commun.) and is illustrated in Figure 1E. No solid evidence of correlation with the chemical zoning of the mineral was found, in spite of the evidence that one of the CL activators is manganese. Despite their position *versus* the contact, the composition of individual crystals is remarkably uniform, with Mn < 0.005 *apfu*, Fe²⁺ < 0.007 *apfu*, and Mg < 0.022 *apfu*.

Garnets

The occurrence and the characteristics of the Ca garnets in the skarn from Cornet Hill were documented in detail by Marinacea *et al.* (2001). Particularly in the exoskarn, small crystals of subhedral grossular (up to 1 mm across) or larger crystals of titanian andradite (up to 8 mm across) occur as accessory minerals in both CH 2 and CH 3 zones. No birefringence anomalies were perceived. Both Ti-poor and Ti-rich grossular (the first and the second generations of garnet described by Marinacea *et al.* 2001) and titanian andradite replacing perovskite were identified and analyzed (Marinacea *et al.* 2001). As a peculiarity, the garnets from the exoskarn zone have a more significant hydrogarnet component

than their counterparts in the endoskarn (see Marinacea *et al.* 2001, for details).

Perovskite

Granular inclusions of perovskite in the spurrite and tilleyite masses are common in most of the samples, and particularly in those containing spurrite. Concentrations of perovskite were observed at the border between the CH 1 and CH 2 zones, where perovskite associates with gehlenite and wollastonite or directly with spurrite. Generally, perovskite occurs as pseudocubic crystals, sometimes twinned, commonly varying in size between 0.01 and 0.05 mm. The crystals have an equant habit (Fig. 1F).

The mineral is colorless in thin section. The physical constants of a selected sample (2160) are $\alpha = 2.302(2)$, $\beta(\text{calc.}) = 2.341(2)$, $\gamma = 2.383(2)$, $2V = 89^\circ$, $D_x = 4.049 \text{ g/cm}^3$, and $D = 4.04(1) \text{ g/cm}^3$.

Unit-cell parameters of three representative samples of perovskite from Cornet Hill were obtained by least-squares refinement of the X-ray powder data and are given in Table 2. They are generally smaller than those refined by Koopmans *et al.* (1983) for the synthetic perovskite [a 5.3829(3), b 5.4458(3), c 7.6453(4) Å, keeping $a < b < c$], which suggests that the (Al, Si)-for-Ti substitutions in natural perovskite, even reduced, could decrease the cell parameters.

Results of EMP analyses of five representative samples of perovskite are given in Table 7. The structural formulae were normalized to 3 (O) *apfu*. As can be observed in the table, the substitutions at the six-fold

coordinated B-site normally occupied by Ti are minor (up to 2.11% Si and 1.20% Al enter the site) as well as the substitutions at the twelve-fold coordinated A-site normally occupied by Ca (up to 0.10% K, 0.20% Na, 0.50% Mg, 0.10% Mn, and 3.26% Fe enter the site); see Koopmans *et al.* (1983) for structure.

Monticellite

Monticellite occurs scarcely in the exoskarn zone from Cornet Hill. The mineral is scattered at random throughout the spurrite and tilleyite masses. The crystals are subhedral, rarely euhedral, with prismatic habit. They average 0.2 mm in length and up to 0.05 mm in width and normally form aggregates isolated in the mass of tilleyite from the CH 3 zone. The mineral does not show any significant chemical or optical zoning. The average chemical analysis obtained as result of five point-analyses performed by EMPA on three different crystals of monticellite from a tilleyite- and wollastonite-bearing sample is (in wt.% of oxides): SiO₂ 37.52, TiO₂ 0.01, Al₂O₃ 0.01, CaO 36.14, MgO 21.20, MnO 0.46, FeO 5.10, Total 100.46. Normalized to 4 (O), this yields the formula: (Ca_{1.033}Mg_{0.843}Mn_{0.010}Fe_{0.114})(Si_{1.000}O₄).

Note that the contents of Al and Ti are too low to appear in the formula, whereas the Ca content is higher than the ideal 1 *apfu*. The compositional formula

that can be deduced includes 87.18 mol.% monticellite, 11.79 mol.% kirschsteinite, and 1.03 mol.% glaucochroite.

Ellestadite-(OH)

Ellestadite-(OH) was first reported at Cornet Hill by Pascal *et al.* (2001) and Marincea *et al.* (2001) who gave short descriptions and a couple of microprobe analyses. It occurs rarely as randomly oriented inclusions in spurrite and tilleyite, but also in gehlenite. Most ellestadite-(OH) in the tilleyite- or spurrite-bearing skarn is found as discrete grains with euhedral to subhedral, prismatic habit (Fig. 1F). Grains can have a maximum length of 0.5 mm with a maximum width of about 0.1 mm. The majority of the ellestadite-(OH) grains in CH 3 zone are directly enclosed within tilleyite (Fig. 1F). The indices of refraction of a representative sample (2173) are: $\epsilon = 1.649(1)$ and $\omega = 1.653(1)$, resulting in a mean refraction index $\bar{n} = (2\omega + \epsilon)/3$ of 1.6517 for use in Gladstone-Dale calculations. The indices of refraction fit well with those given for ellestadite-(OH) by Harada *et al.* (1971). The mean density of the same sample was measured by the sink-float method, at 25 °C, using a mixture of methylene iodide and toluene as the immersion liquid. The average of three determinations yielded $D_m = 3.03(1)$ g/cm³, which compares well with

TABLE 7. REPRESENTATIVE ELECTRON-MICROPROBE COMPOSITIONS OF PEROVSKITE, CORNET HILL*

Sample	2160	2176	CH49	CH51	CH78
N ⁽¹⁾	4	4	3	2	2
Zone	CH 2	CH 2	CH 2	CH 3	CH 3
SiO ₂	0.92	0.15	0.09	0.04	0.58
TiO ₂	56.41	58.24	57.36	57.14	57.08
Al ₂ O ₃	0.33	0.17	0.21	0.25	0.46
FeO ⁽²⁾	1.51	1.01	1.28	1.72	0.42
MnO	0.07	0.00	0.03	0.00	0.00
MgO	0.08	0.01	0.00	0.02	0.14
CaO	40.46	40.24	40.39	39.66	40.39
Na ₂ O	0.04	0.02	0.02	0.01	0.02
K ₂ O	0.00	0.04	0.01	0.00	0.00
Total	99.82	99.88	99.39	98.84	99.09
Number of cations on the basis of 3 (O)					
Si	0.021	0.003	0.002	0.001	0.013
Ti	0.963	0.994	0.986	0.988	0.978
Al	0.009	0.005	0.006	0.007	0.012
Fe ²⁺	0.029	0.019	0.024	0.033	0.008
Mn	0.001	0.000	0.001	0.000	0.000
Mg	0.003	0.000	0.000	0.001	0.005
Ca	0.985	0.978	0.989	0.977	0.986
Na	0.002	0.001	0.001	0.000	0.001
K	0.000	0.001	0.000	0.000	0.000

* Results expressed in wt.%; (1) number of point analyses; (2) total iron as FeO.

TABLE 8. REPRESENTATIVE ELECTRON-MICROPROBE COMPOSITIONS OF HYDROXYELLESTADITE, CORNET HILL*

Sample	2178	CH49	2300	2159	2173	2233	2316A	2316B	CH51
N ⁽¹⁾	3	9	3	8	6	2	5	5	6
Zone	CH 2	CH 2	CH 3						
SiO ₂	19.99	15.57	18.33	18.12	17.57	18.43	17.72	17.45	17.33
SO ₃	20.21	21.05	19.86	23.01	24.04	21.90	20.93	21.14	21.96
P ₂ O ₅	1.04	5.38	2.95	0.79	0.40	1.12	2.37	2.84	2.61
Al ₂ O ₃	0.02	0.03	0.00	0.01	0.01	0.01	0.02	0.02	0.03
CaO	54.56	55.58	54.67	54.42	53.72	55.52	54.52	54.43	56.01
MgO	0.00	0.00	0.01	0.01	0.01	0.02	0.02	0.01	0.01
MnO	0.06	0.04	0.04	0.01	0.06	0.01	0.04	0.02	0.03
FeO ⁽²⁾	0.03	0.17	0.00	0.03	0.02	0.06	0.05	0.10	0.05
Na ₂ O	0.68	0.23	0.21	0.28	0.64	0.43	0.58	0.49	0.27
K ₂ O	0.03	0.03	0.00	0.01	0.01	0.01	0.07	0.02	0.02
F	0.22	0.25	0.63	0.50	0.37	0.27	0.51	0.57	0.80
Cl	0.27	0.09	0.51	0.34	0.40	0.40	0.31	0.32	0.39
H ₂ O ⁽³⁾	2.60	1.58	2.09	2.03	1.94	1.76	1.71	1.84	1.33
O = F,Cl	99.71	100.00	99.30	99.56	99.19	99.94	98.85	99.25	100.84
Total	- 0.15	- 0.13	- 0.38	- 0.29	- 0.25	- 0.20	- 0.29	- 0.31	- 0.43
	99.56	99.87	98.92	99.27	98.94	99.74	98.56	98.94	100.41
Number of cations on the basis of 3 (Si + S + P) and 13 (O + OH + F + Cl)									
Si	1.664	1.300	1.539	1.508	1.466	1.544	1.500	1.466	1.443
S ⁶⁺	1.263	1.320	1.251	1.437	1.506	1.376	1.330	1.332	1.373
P	0.073	0.380	0.210	0.055	0.028	0.080	0.170	0.202	0.184
Al	0.002	0.003	0.000	0.001	0.001	0.001	0.002	0.002	0.003
Ca	4.867	4.972	4.918	4.852	4.803	4.983	4.947	4.899	4.999
Mg	0.000	0.000	0.001	0.001	0.001	0.003	0.003	0.001	0.001
Mn	0.004	0.003	0.003	0.001	0.004	0.001	0.003	0.001	0.002
Fe ²⁺	0.002	0.011	0.000	0.002	0.001	0.004	0.004	0.007	0.003
Na	0.109	0.036	0.034	0.045	0.104	0.070	0.095	0.080	0.044
K	0.003	0.003	0.000	0.001	0.001	0.001	0.008	0.002	0.002
F	0.059	0.066	0.167	0.132	0.097	0.071	0.135	0.151	0.212
Cl	0.038	0.012	0.073	0.048	0.056	0.057	0.044	0.046	0.055
(OH) ⁻	1.440	0.882	1.170	1.130	1.079	0.984	0.968	1.033	0.738

* Results expressed in wt.%; (1) number of point analyses; (2) total iron as FeO; (3) as calculated for charge balance.

the calculated density based on the chemical formula (Table 8) and unit-cell parameters (Table 2), with $Z = 2$ [Harada *et al.* (1971) gave $Z = 1$ for a 26 (O,OH,F,Cl)-based chemical formula]; $D_m = 3,047 \text{ g/cm}^3$.

Gladstone-Dale calculations give $K_p = 0.2139$ and $K_c = 0.2038$, for a compatibility index of -0.049 , indicating good agreement between the physical and chemical data (Mandarino 1981).

The results of EMP analyses of nine representative samples of ellestadite-(OH) from Cornet Hill are given in Table 8. The composition of each crystal is fairly uniform, although some crystals show slight variations in P versus Si and S content. As can be seen in the Table 8, phosphate (0.93 to 12.67% from the tetrahedral groups) also enters into the structure. Analyses give consistently low totals, in spite of the calculation of water, which probably implies the substitution $(\text{CO}_3\text{OH})^{3-}$ -for- $(\text{SO}_4)^{2-}$ (e.g., Harada *et al.* 1971). The formulae were, however, calculated on the basis of 3

(Si + S + P) and 13 (O + OH + F + Cl), ignoring the eventuality of this substitution.

In terms of the three four-fold coordinated cations, Si, S, and P, the samples from the CH 1 zone plot in the Si-bearing apatite field, whereas samples from CH 2 and CH 3 plot in the ellestadite-(OH) field. The most common compositional variations of ellestadite-(OH) from the exoskarn zone (Table 8) are conveniently represented on the ternary diagram in Figure 3. All but two of the samples analyzed could be characterized as S- and P-substituted silicates, and all the plots in Figure 3 proving an excellent agreement with the assumption of Rouse & Dunn (1982) that the Si:S ratio in ellestadite is nearly 1:1.

As a remark, halogens occupy between 6.31 and 26.57% of the anion site.

X-ray powder diffraction data refined for a selected sample of ellestadite-(OH) in space group $P6_3/m$ yielded the unit-cell parameters given in Table 2. The c cell parameter is slightly larger than that reported by Harada

et al. (1971) for the type material from Chichibu Mine, Japan (6.930 Å *versus* 6.921 Å) suggesting a lower P content in our sample (*e.g.*, Neubauer & Pöllmann 1995).

Vesuvianite

Vesuvianite, sometimes pseudomorphous after gehlenite, occurs locally in the exoskarn assemblages, being the result of lower temperature hydrothermal activity (Marincea *et al.* 2001).

Vesuvianite from the exoskarn zone occurs both as euhedral crystals up to 1 cm across and as anhedral, amoeba-like pods that engulf gehlenite. The birefringence of the crystals is characteristically very low and some grains are nearly isotropic, suggesting high OH content (Fig. 1G, *e.g.*, Deer *et al.* 1986). This is consistent with the chemical data offered by Marincea *et al.* (2001), who gave a more comprehensive description.

DATA FOR NEW SECONDARY MINERALS

The secondary minerals from Cornet Hill, resulting from hydrothermal and weathering processes, were documented in detail by Marincea *et al.* (2001), so their description will not be repeated. Three new secondary species were, however, identified during this study and will be briefly described: afwillite, thaumasite, and fukalite.

Afwillite

Afwillite is the main alteration product of spurrite, occurring as thin crusts or veins along the cracks of spurrite masses, where calcite is often associated. Microscopically, the mineral appears as small masses of interlaced prisms, or parallel growth prismatic acicular or fibrous crystals lining veins that cut across the mass of spurrite (Fig. 1H). It was not possible to obtain reli-

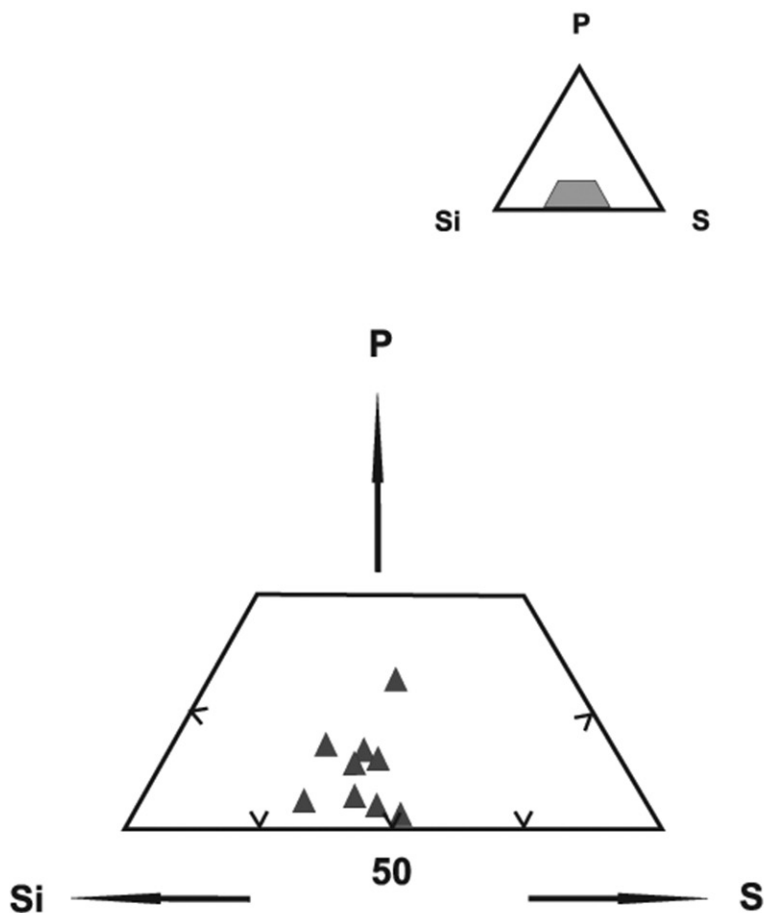


FIG. 3. Ternary diagram showing the position of ellestadite-OH samples from Cornet Hill in the P-Si-S system. Note that all of the plots are close to Si = S bisectrix.

able optical parameters because of the grain size and fibrous character of the mineral. A mean refractive index of 1.625 was obtained from a group of crystals.

Results of averaged EMP analyses from afwillite grains from three different thin sections are given in Table 9. The water content was calculated for the charge balance, using the chemical formula confirmed by Malik & Jeffery (1976). As well as in the replaced spurrite, the Mn-, Mg-, Fe²⁺-, Na-, and K-for-Ca substitutions are minor (Table 9).

The unit-cell parameters of a selected sample, refined by least squares on the basis of the X-ray powder data, assuming a monoclinic cell, space group *Cc*, are given in Table 2. They are virtually identical to the unit-cell parameters given by Malik & Jeffery (1976) for afwillite from the type locality, *i.e.*, *a* 16.278(1), *b* 5.6321(4), *c* 13.236(1) Å, and β 134.898(3)°.

Thaumasite

Thaumasite occurs in veinlets, a few tens of μm wide, that cut spurrite crystals and locally fill cleavages and crack in the crystals; rarely, thaumasite occurs as rims on ellestadite-(OH) grains. The thaumasite needles tend to be extensively intergrown, giving rise to fan-shaped or interwoven aggregates. Felted crusts of silky fibers that line fractures in the spurrite mass also occur. The indices of refraction measured for a selected sample as minimum and maximum values are $\epsilon = 1.468(1)$ and $\omega = 1.505(1)$.

The chemical composition of the same sample, obtained as mean of three point analyses, is (in wt.% oxides): SiO₂ 9.80, CaO 26.92, MnO 0.04, FeO 0.10, SO₃ 12.28, P₂O₅ 0.41, CO₂ 7.05 (as calculated for C = 1 *apfu*), H₂O (calculated) = 43.24, F = 0.12 (O = F = -0.05), Cl = 0.10 (O = Cl = -0.02), Total = 99.99. The chemical-structural formula calculated on the basis of 6 (O, OH, F) and 7 (O) atoms *pfu*

TABLE 9. REPRESENTATIVE ELECTRON-MICROPROBE COMPOSITIONS OF FUKALITE AND AFWILLITE, CORNET HILL*

Sample	2162 ⁽¹⁾	2259 ⁽¹⁾	P 55 ⁽¹⁾	2162 ⁽²⁾	2259 ⁽²⁾	2315 ⁽²⁾
N ⁽³⁾	3	3	3	3	6	13
SiO ₂	29.44	29.47	29.52	35.00	34.98	34.89
TiO ₂	0.09	0.01	0.00	0.06	0.05	0.05
Al ₂ O ₃	0.01	0.03	0.07	0.01	0.03	0.16
CaO	55.08	55.12	55.06	49.00	48.96	48.81
MgO	0.00	0.02	0.05	0.03	0.03	0.16
MnO	0.07	0.07	0.03	0.05	0.06	0.06
FeO ⁽⁴⁾	0.02	0.03	0.00	0.02	0.03	0.05
Na ₂ O	0.01	0.02	0.01	0.05	0.03	0.02
K ₂ O	0.00	0.01	0.02	0.01	0.02	0.01
CO ₂ ⁽⁵⁾	10.78	10.79	10.81	-	-	-
H ₂ O ⁽⁵⁾	4.36	4.43	4.43	15.77	15.67	15.74
F	0.14	0.00	0.00	0.00	0.14	0.05
O = F	-0.06	-	-	-	-0.06	-0.02
Total	99.94	100.00	100.00	100.00	99.94	99.98
Number of cations on the basis of „X” (O, OH, F) ⁽⁶⁾						
Si	1.995	1.995	1.997	1.995	1.994	1.988
Ti	0.005	0.001	0.000	0.003	0.002	0.002
Al	0.001	0.002	0.006	0.001	0.002	0.011
Ca	3.997	3.996	3.990	2.993	2.996	2.983
Mg	0.000	0.003	0.005	0.003	0.003	0.014
Mn	0.004	0.004	0.002	0.002	0.003	0.003
Fe ²⁺	0.001	0.002	0.000	0.001	0.001	0.002
Na	0.001	0.003	0.001	0.006	0.003	0.002
K	0.000	0.001	0.003	0.001	0.001	0.001
C	0.998	0.999	0.999	-	-	-
(OH) ⁻	1.970	2.000	2.000	6.000	5.975	5.991
F	0.030	0.000	0.000	0.000	0.025	0.009

* Results expressed in wt.%; totals were recalculated at 100% without considering O = F; (1) fukalite; (2) afwillite; (3) number of point analyses; (4) total iron as FeO; (5) as calculated for stoichiometry; (6) X = 11 (O, OH, F) and 7 cations other than H⁺ for fukalite, and X = 10 (O, OH, F) for afwillite.

is $(\text{Ca}_{2.994}\text{Mn}_{0.004}\text{Fe}_{0.009})\text{Si}_{1.017}(\text{S}_{0.957}\text{P}_{0.036})\text{C}_{0.999}\text{O}_7(\text{OH}_{5.943}\text{F}_{0.039}\text{Cl}_{0.018}) \cdot 12\text{H}_2\text{O}$.

The cell parameters obtained for a selected sample of thaumasite from Cornet Hill are given in Table 2. They compare well with those determined by single crystal diffractionmetry for the Långban thaumasite by Effenberger *et al.* (1983): *a* 10.030(7) and *c* 10.396(6) Å.

Fukalite

Interstitial grains of fukalite were found as inclusions in large masses of tilleyite in a few samples. The individual crystals do not exceed 30 µm in their longest dimension and have prismatic habit. Due to the superposition with lines pertaining to tilleyite, the XRD study was difficult; the unit-cell parameters given in Table 2 were consequently refined on the basis of a few reflections unequivocally attributable to fukalite. For this reason, it was impossible to identify the polytype; the optical study favors, however, the hypothesis of an orthorhombic symmetry. The mineral is biaxial positive, with 2V of 90°. Because of the small dimensions of the crystals, no reliable refraction indices were measured.

The unit-cell parameters given in Table 2 were calculated assuming orthorhombic symmetry, space group *Bmmb*, as proposed by Henmi *et al.* (1977) for fukalite from the type locality. The obtained values fit well with those obtained for orthorhombic polytypes by both Henmi *et al.* (1977; *a* 5.48, *b* 3.78, *c* 23.42 Å) for fukalite from the type locality and by Merlino *et al.* [2009; *a* 5.47(1), *b* 3.784(2), *c* 23.38(2) Å] for fukalite from the Gumeshevsk deposit, in Russia.

The average results of nine point analyses performed on fukalite crystals from three different thin sections are given in Table 9. The data obtained herein differ substantially from those given by Henmi *et al.* (1977) for fukalite from the type locality, because of the noticeable deficiency in F, most likely due to the replacement of this element by (OH), as in the case of fukalite from Gumeshevsk (Merlino *et al.* 2009).

Further examination of fukalite from Cornet Hill is necessary and is in progress.

GENETIC CONSIDERATIONS

As stated by Marincea *et al.* (2001), the initial mineral associations crystallized during the metasomatic events at Cornet Hill were affected by three subsequent stages of hydrothermal alteration and weathering. In the exoskarn zone, prograde metasomatism resulted in the crystallization of tilleyite and spurrite with accessory wollastonite, gehlenite, perovskite, grossular, monticellite, and ellestadite-(OH). Apparently, regressive alteration of spurrite into tilleyite, as mentioned by Reverdatto *et al.* (1980) at the outer contact of the Anakite dolerite massif (Siberia), is limited or absent, both minerals altering to afwillite and fukalite, probably

at the same time as gehlenite alters to vesuvianite. The breakdown of tilleyite into spurrite and carbon dioxide (Bowen 1940) seems quite reduced, if existent. In fact, the normal development of a sequence of wollastonite → tilleyite → spurrite type, that fits with a progressive increasing of temperature and decreasing CO₂ pressure (Zharikov & Shmulovich 1969), was highly perturbed, in the exoskarn zone, by the important local variations of the CO₂ and H₂O activities due to pronounced decarbonation and dehydration reactions. More likely is a reversed sequence, of the spurrite → tilleyite type (Pascal *et al.* 2001).

Estimates for the lithostatic pressure during emplacement of the Cornet Hill pluton, based on the actual thickness of the sequence of thrustured Mesozoic ophiolites and of Neojurassic marbles in the cover, are about 1 kbar. There is no compelling argument to indicate that load pressure equaled fluid pressure during the exoskarn formation. If pressure equilibrium was not so important during the contact metamorphism and skarn formation, fluid pressures would be lower than the lithostatic ones. Pascal *et al.* (2001) estimated, on the basis of mineral equilibria, that the CO₂ pressure was very low (up to 16 bars) and the H₂O pressure was less than 0.75 kbar. Thus there is considerable uncertainty regarding the estimate of fluid pressures during skarn formation, although pressures less than 1 kbar seem assured.

The peak temperature in this context is clearly lower than 820 °C, since the presence of unreacted spurrite in direct contact with monticellite supposes that the temperature was too low to permit the reaction 2 monticellite + spurrite = 2 merwinite + calcite that may initiate at this temperature (Joesten 1976). In this context, a peak temperature of about 710 °C, as estimated by Pascal *et al.* (2001), seems reasonable.

The exoskarn from Cornet Hill has clearly undergone a late metasomatic event which produced diopside veins cross-cutting tilleyite and spurrite (Pascal *et al.* 2001), titanian andradite replacing perovskite, small masses and veins of vesuvianite replacing gehlenite, *etc.* As shown by Marincea *et al.* (2001), subsequent hydrothermal and weathering overprint on the primary assemblages resulted in the formation of three secondary parageneses: (1) an early hydrothermal one that includes afwillite, fukalite, thaumasite, scawtite, xonotlite, and hibschite; (2) a late hydrothermal one that includes 11 Å tobermorite, riversideite, thomsonite, gismondine, aragonite, and calcite; and (3) a weathering paragenesis that includes plombièrite, portlandite, and allophane.

ACKNOWLEDGEMENTS

The Rhône-Alpes Region is gratefully acknowledged for financing the beginning of this research work by via a TEMPra grant to the senior author in 1999-2000. The development of the study was possible due to the financial help of the National Authority for

Scientific Research in Romania through the projects 31-030/2007, 91-017/2007, 58/2008, and PN-II-ID-PCE-2011-3-0023. The research was also supported by the co-operative MECI-CGRI research program between the Romanian and Walloon Governments under Project 2.11/2007. Thanks are due to Messrs. Hubert Rémy, Michel Fialin, and to Mrs. Claudine Richard (CNRS, France) for advising on the use of the electron microprobe, to Mr. Jean Naud (Université Catholique de Louvain), for part of the X-ray powder diffraction work, to Mrs. Raymonde Gibert (Ecole Nationale Supérieure des Mines, Saint Etienne) for the infrared records, and to Mr. Régis Piret (Université Catholique de Louvain), who kindly communicated some of the XRD and EMP analyses used for this study. We express our thanks to Dr. Hans-Peter Schertl (University of Bochum) for providing excellent supplementary EMP analyses. Fruitful discussions on the field with Jean Verkaeren, Marie-Lola Pascal, Essaid Bilal, Evgheny Galuskin, Irina Galuskina, Gheorghe Ilinca, Robert Martin, and Régis Piret are highly appreciated. The authors are grateful to the Associate Editor Yuanming Pan and to Editor Lee A. Groat for handling the manuscript, as well as to Dr. Joel Grice and to an anonymous referee for their thorough reviews of an earlier draft.

REFERENCES

- APPLEMAN, D.E. & EVANS, H.T., JR. (1973) Indexing and least-squares refinement of powder diffraction data. *Geological Survey, Computer Contribution* **20**, (NTIS Doc. PB-216).
- BENOIT, P.H. (1987) Adaptation to microcomputer of the Appleman-Evans program for indexing and least-squares refinement of powder-diffraction data for unit-cell dimensions. *American Mineralogist* **72**, 1018-1019.
- BOWEN, N.L. (1940) Progressive metamorphism of siliceous limestone and dolomite. *Journal of Geology* **48**, 225-274.
- DEER, W.A., HOWIE, R.A., & ZUSSMAN, J. (1986) *Rock-forming minerals, Volume 1B, Disilicates and ring silicates, 2nd edition*. Longman Ed., Avon, U.K., (629pp).
- EFFENBERGER, H., KIRFEL, A., WILL, G., & ZOBETZ, E. (1983) A further refinement of the crystal structure of thaumasite, $\text{Ca}_3\text{Si}(\text{OH})_6\text{CO}_3\text{SO}_4 \cdot 12\text{H}_2\text{O}$. *Neues Jahrbuch für Mineralogie (Monatshefte)* **1**, 60-68.
- GRICE, J.D. (2005) The structure of spurrite, tilleyite and scawtite, and relationships to other silicate-carbonate minerals. *Canadian Mineralogist* **43**, 1489-1500.
- HARADA, K., NAGASHIMA, K., NAKAO, K., & KATO, A. (1971) Hydroxyllellastadite, a new apatite from Chichibu Mine, Saitama Prefecture, Japan. *American Mineralogist* **56**, 1507-1518.
- HENMI, C., KUSACHI, I., KAWAHARA, A., & HENMI, K. (1977) Fukalite, a new calcium carbonate silicate hydrate mineral. *Mineralogical Journal* **8**, 374-381.
- ISTRATE, G., ȘTEFAN, A., & MEDEȘAN, A. (1978) Spurrite and tilleyite in the Cornet Hill, Apuseni Mountains, Romania. *Revue Roumaine de Géologie, Géophysique et Géographie - Série de Géographie* **22**, 143-153.
- JOESTEN, R. (1976) High-temperature contact metamorphism of carbonate rocks in a shallow crustal environment, Christmas Mountains, Big Bend region, Texas. *American Mineralogist* **61**, 776-781.
- KONEV, A., PASERO, M., PUSHCHAROVSKY, D., MERLINO, S., KASHAEV, A., SUVOROVA, L., USHCHAPOVSKAYA, Z., NARTOVA, N., LEBEDEVA, Y., & CHUKANOV, N. (2005) Biraite-(Ce), $\text{Ce}_2\text{Fe}^{2+}(\text{CO}_3)(\text{Si}_2\text{O}_7)$, a new mineral from Siberia with a novel structure type. *European Journal of Mineralogy* **17**, 715-721.
- KOOPMANS, H.J.A., VAN DE VELDE, G.M.H., & GELLINGS, P.J. (1983) Powder neutron diffraction studies of the perovskites CaTiO_3 and CaZrO_3 . *Acta Crystallographica C* **39**, 1323-1325.
- The Infrared Spectra of Minerals (V.C. Farmer, ed.). Mineralogical Society Monograph, London, U.K. (69-85).
- LOUISNATHAN, S.J. & SMITH, J.V. (1970) Crystal structure of tilleyite: refinement and coordination. *Zeitschrift für Kristallographie* **132**, 288-306.
- LUPU, M., AVRAM, E., ANTONESCU, E., DUMITRICĂ, P., LUPU, D., & NICOLAE, I. (1993) The Neojurassic and the Cretaceous of the Drocea Mts.: The stratigraphy and the structure of an ensialic marginal basin. *Romanian Journal of Tectonics and Regional Geology* **75**, 53-66.
- MALIK, K.M.A. & JEFFERY, J.W. (1976) A re-investigation of the structure of awillite. *Acta Crystallographica B* **32**, 475-480.
- MANDARINO, J.A. (1981) The Gladstone-Dale relationship. IV. The compatibility concept and its application. *Canadian Mineralogist* **19**, 441-450.
- MARINCEA, Ș., BILAL, E., VERKAEREN, J., PASCAL, M.L., & FONTEILLES, M. (2001) Superposed parageneses in the spurrite-, tilleyite-, and gehlenite-bearing skarns from Cornet Hill, Apuseni Mountains, Romania. *Canadian Mineralogist* **39**, 1435-1453.
- MARINCEA, Ș., DUMITRAȘ, D.G., GHINEȚ, C., FRANSOLETT, A.-M., HATERT, F., & RONDEUX, M. (2011) Gehlenite from three occurrences of high-temperature skarns, Romania: new mineralogical data. *Canadian Mineralogist* **49**, 1001-1014.
- MERLINO, S., BONACCORSI, E., GRABEZHEV, A.I., ZADOV, A.E., PERTSEV, N.N., & CHUKANOV, N.V. (2009) Fukalite: An example of an OD structure with two-dimensional disorder. *American Mineralogist* **94**, 323-333.
- NEUBAUER, J. & PÖLLMANN, H. (1995) Solid solution series of silico - sulphate - chloride - apatites. *Neues Jahrbuch für Mineralogie (Abhandlungen)* **168**, 237-258.

- PASCAL, M.-L., FONTEILLES, M., VERKAEREN, J., PIRET, R., & MARINCEA, Ș. (2001) The melilite-bearing high-temperature skarns of the Apuseni Mountains, Carpathians, Romania. *Canadian Mineralogist* **39**, 1405-1434.
- PIRET, R. (1997) *Minéralogie et géochimie des skarns de haute température des régions de Măgureaua Vaței et de Cornet Hill (Monts Apuseni)*. Unpublished. M. Sc. Thesis, Université Catholique de Louvain, Belgium.
- POUCHOU, J.L. & PICOIR, F. (1985) PAP ϕ (ρZ) procedure for improved quantitative microanalysis. In *Microbeam analysis* (J.T. Armstrong, ed.). San Francisco Press, San Francisco, U.S.A. (104-106).
- REVERDATTO, V.V. (1970) Pyrometamorphism of limestones and the temperature of basaltic magmas. *Lithos* **3**, 135-143.
- REVERDATTO, V.V., PERTSEV, N.N., & KOROLYUK, V.N. (1980) Zoning of melilite grains as an indicator of regressive evolution of metamorphic process in carbonate-bearing rocks. In *Inhomogeneity of minerals & crystal growth*. Proceedings of the XI General Meeting of IMA, Novosibirsk, 4-10 September, 1978, (59-65) (in Russian).
- ROSS, S.D. & GOLDSMITH, J. (1964) Factors affecting the infrared spectra of planar anions with D_{3h} symmetry. I. Carbonates of the main group and first row transition elements. *Spectrochimica Acta* **20**, 781-784.
- ROUSE, R.C. & DUNN, P.J. (1982) A contribution to the crystal chemistry of ellestadite and the silicate sulfate apatites. *American Mineralogist* **67**, 90-96.
- RUBENACH, M.J. & CUFF, C. (1985) The occurrence of coarse-grained massive tilleyite in the Redcap Creek magmatic skarn, North Queensland. *Mineralogical Magazine* **49**, 71-75.
- SMITH, J.V. (1953) The crystal structure of tilleyite. *Acta Crystallographica* **6**, 9-18.
- SMITH, J.V., KARLE, I.L., HAUPTMAN, H., & KARLE, J. (1960) The crystal structure of spurrite, $Ca_5(SiO_4)_2CO_3$. II. Description of structure. *Acta Crystallographica* **13**, 454-458.
- ȘTEFAN, A., LAZĂR, C., BERBELEAC, I., & UDUBAȘA, G. (1988) Evolution of the Banatitic magmatism in the Apuseni Mts. and the associated metallogenesis. *Dari de Seama ale Sedintelor Institutului de Geologie si Geofizica* **72-73/2**, 195-213.
- TILLEY, C.E. (1929) On larnite (calcium orthosilicate, a new mineral) and associated minerals from the limestone contact-zone of Scawt Hill, Co. Antrim. *Mineralogical Magazine* **22**, 77-86.
- TILLEY, C.E. (1938) On scawtite pseudomorphs after spurrite at Scawt Hill, Co. Antrim. *Mineralogical Magazine* **35**, 38-40.
- WHITE W.B. (1974) The carbonate minerals. In *The infrared spectra of minerals* (V.C. Farmer, ed.). Mineralogical Society Monograph 4, London, U.K. (227-284).
- ZHARIKOV, V.A. & SHMULOVICH, K.I. (1969) Experimental study of the system $CaO-SiO_2-CO_2$ between 800-1100°C and at $P_{CO_2} = 50-500$ kg/cm². *Doklady Akademii Nauk* **188**, 170-173 (in Russian).

Received June 11, 2012, revised manuscript accepted May 2, 2013.

